Strain and bond length dynamics upon growth and transfer of graphene by NEXAFS spectroscopy from first principles and experiment

Rojas, Wudmir; Winter, Allen; Grote, James; Kim, S.S.; Naik, Rajesh R. ; Williams, A.D.; Weiland, Conan; Principe, Edward; Fischer, D.A.; Banerjee, Sarbajit; Prendergast, D.; Campo, Eva

Langmuir

DOI:
10.1021/acs.langmuir.7b03260

Published: 01/01/2018

Peer reviewed version

LANGMUIR

Subscriber access provided by NATL SCIENCE FOUNDATION

Article

Strain and bond length dynamics upon growth and transfer of graphene by NEXAFS spectroscopy from first principles and experiment

Wudmir Yudy Rojas, Allen Douglas Winter, James Gerard Grote, Steve S. Kim, Rajesh R. Naik, Adrienne D. Williams, Conan Weiland, Edward Principe, Daniel A Fischer, Sarbajit Banerjee, David Prendergast, and Eva M. Campo

Langmuir, **Just Accepted Manuscript** • DOI: 10.1021/acs.langmuir.7b03260 • Publication Date (Web): 29 Dec 2017

Langmuir is published by the American Chemical Society. 1155 Sixteenth Street N.W., Washington, DC 20036

Strain and bond length dynamics upon growth and transfer of graphene by NEXAFS spectroscopy from first principles and experiment

*W. Y. Rojas[1], A. D. Winter[1], J. Grote[2], S.S. Kim[2], R.R. Naik[2], A. D. Williams[2], C. Weiland[3], E. Principe[3], D. A. Fischer[4], S. Banerjee[5], D. Prendergast[6], E. M. Campo[1, 7 *]*

[1] School of Electronic Engineering, Bangor University, Bangor LL57 1UT, UK.

[2] Materials and Manufacturing Directorate, Air Force Research Laboratory, Wright-Patterson AFM, Ohio 45433, USA.

[3] Synchrotron Research Inc, Melbourne, FL 32901, USA

[4] National Institute of Standards and Technology, Gaithersburg, Maryland 20899, USA.

[5]Departments of Chemistry and Materials Science and Engineering, Texas A&M University, College Station, Texas 77842-3012, USA.

[6] The Molecular Foundry, Materials Science Division, Lawrence Berkeley National Laboratory, Berkeley, California 94720, USA.

[7] Department of Physics and Astronomy, University of Texas at San Antonio, TX 78249, USA.

As the quest towards novel materials proceeds, improved characterization technologies are needed. In particular, the atomic thickness in graphene and other 2D materials renders some conventional technologies obsolete. Characterization technologies at wafer level are needed with enough sensitivity to detect strain in order to inform fabrication. In this work, NEXAFS spectroscopy was combined with simulations to predict lattice parameters of graphene grown on copper and further transferred to a variety of substrates. The strains associated with the predicted lattice parameters are in agreement with experimental findings. The approach presented here holds promise to effectively measure strain in graphene and other 2D systems at wafer levels to inform manufacturing environments.

Introduction

Augmenting needs in processing speed and memory storage amongst others pave the way to post-CMOS technologies, where materials discovery has long been identified as a limiting factor given the inability of current gate and dielectric materials to yield improved mobilities while maintaining a device switching ability.[1] A remedial approach by the Materials Genome Initiative has identified graphene as a key material system suitable to be studied under a predictive materials science approach,[2] i.e. Materials by Design, to effectively inform industry by closing up the theory/experiment/data paradigm.[3]

Graphene - a 2D layer of single carbon atom thickness arranged in a honeycomb lattice-has attracted great interest owing to exceptional electrical properties at room temperature, as first reported in 2004.[4] In this scheme, mobilities in graphene have been quoted as high as 40-70k $cm^2V^{-1}s^{-1}$.[1] Since then, novel concepts towards electronic and optoelectronic devices have been reported.[5] Graphene obtained by graphite exfoliation has been successfully used for proof of concept device applications.[4] However, grand challenges exist for industrial-scale fabrication of

large-area, defect-free graphene under controlled conditions and onto a desired substrate to produce electronic devices such as graphene- based field effect transistors (GFETs).[6] Some of these challenges revolve around in plane and out of plane defects resulting from processing that induce random strain fluctuations, which have been identified as the dominant disorder source in graphene devices.[7]

Indeed, strain and rippling effects, i.e. in and out of plane strain,[7] both generated early on during growth prior to any processing, mostly as a result of thermal mismatch between metal substrates and graphene.[8] In addition, graphene growth has been reviewed recently to emphasize the growth dynamics at the atomistic level on all metallic and SiC substrates, where a wealth of intrinsic defects –beyond strain- such as dislocations and vacancies readily nucleate from growth.[9] Albeit, despite great success of graphene synthesis on Cu foils by CVD techniques[10, 11] in the last years to produce large area graphene at low cost, the quality of these films is typically beneath that of epitaxially-grown graphene on SiC.[12] This is promoting research to devise efficient methods to enable graphene transfer with higher fidelity.[13] Improved transfer approaches aim at minimizing structural defects, such as growth-derived mechanical strain and ripples (responsible for in and out of plane strain as mentioned above), as well as impurities, adsorbed atoms or molecules from transfer mechanisms, as well as transfer-derived mechanical effects.[14, 15]

The deleterious interplay between morphology and electronic properties in graphene has been recently explored.[16] Indeed, a detailed account of the electronic conductivity of graphene in scenarios whose degree of corrugation varied from wide (135 nm) to narrow (16nm) wrinkles with heights up to 6 nm was recently provided by Zhu et al.[16] In particular, post processing promoted conventional ripples to standing, collapsed and folded wrinkle morphologies, all with

specific electronic transport attributes. Albeit, some reports have highlighted the advantages of such corrugated graphene layers as they improve on charge storage enhancement, strain sensitivity, and chemical reactivity enhancement inclusive of band-gap opening.[17] Clearly, these properties are the subject of current studies to be leveraged in suitable applications. Indeed, mechanical effects resulting from growth and processing have been the object of much attention recently; where ripples, wrinkles and crumples become newly defined morphologies resulting from intrinsic thermal fluctuation, thermal expansion and pre-stretched substrates whose dimensions range on the 0.1-10 nm, 100 nm-1 μm, and above 1 μm respectively.

On the characterization end, a number of techniques have been employed to describe and quantify the extent of mechanical deformation in graphene, such as Transmission Electron Microscopy (TEM) and Scanning Tunnel Microscopy (STM) on the morphological end and Low Energy Electron Diffraction (LEED), Raman, and Synchrotron spectroscopies on the spectroscopic end.[9] In particular, the value of Near Edge X-ray Absorption Fine Structure (NEXAFS) spectroscopy has been recently highlighted to study graphene.[18] NEXAFS spectroscopy is a synchrotron technique, which consists on the excitation of a core electron to an unoccupied antibonding state.[19] Information on molecular orientation and chemistry can be obtained.[20-22] On those lines, corrugations and doping in CVD-grown graphene on Cu have been investigated effectively by theoretical and experimental NEXAFS analysis, as well as interface chemical bonding of single layer graphene (SLG) deposited on Cu, Ni and Co substrates. [23-25] Earlier, some of the authors had successfully used experimental NEXAFS to widely explore rippling and interactions at interfaces of single and bilayer graphene growth on Cu by chemical vapor deposition (CVD) and transferred to SiO_2 substrates.[18]

In this paper, we complement those initial studies through a hybrid theoretical/experimental approach, by analyzing strain effects on the lattice parameter resulting from growth and subsequent transfer to foreign substrates. In this scheme, with the aid of theoretical standards calculated through first principles, lattice constants of transferred graphene are predicted as well as average strains, by virtue of relationship between bond lengths and σ* shifts in NEXAFS spectroscopy. Indeed, early on Molecular Orbital calculations had showed that the σ* positions of atoms were dependent on bond lengths.[26] In this scheme, a strained bond yields a shift to lower σ* energy positions that can be recorded for the differently processed samples. To this end, a total of six experimental samples and seven theoretical samples will be studied, as described in the methodology description in the experimental section.

The approach presented here is an alternative to Raman techniques to measure strain effects. Like Raman,[27, 28] the present approach is suitable to deployment in Cu derived graphene, given the low charge transfer between substrate and epilayer, as will be demonstrated. In advantage of Raman technologies, and owing to the advent of large area hyperspectral detectors,[29, 30] this technique is applicable to large substrates at wafer scale, with micro-meter resolution. The combined experimental/theoretical approach featured in this study follows a Materials by Design paradigm, and aims at addressing a pending issue in the context of post-CMOS technologies, as has been described in policy-prompted communications. Lastly, this approach could be useful to other 2D contenders. Moreover, it can be deployed at wafer scale and hence, is prone to industrial-level assessment.

Experimental section

Methodology

Indeed, we have made use of *ab initio* calculations to produce free standing and Cu-conformed mathematical graphene standards with varying degrees of deformation. Along these lines, free-standing graphene (SLG) samples of 2.42 Å, 2.47 Å and 2.51 Å lattice parameters were modeled to probe into the tensile/compressive deformation of the typically reported 2.46 Å CVD grown on Cu.[31] Mathematical graphene samples will be compared to six experimental systems: CVD-grown graphene on Cu (CVD SLG/Cu), epitaxially-grown graphene on SiC, as well as single and four monolayers graphene grown via CVD on Cu, and subsequently transferred to both silicon- and carbon-terminated SiC (SLG/SiC-Si, SLG/SiC-C, 4LG/SiC-Si, 4LG/SiC-C).

Following similar arguments used in earlier publication of one of the authors from the the present work,[32] this experimental design will establish a baseline in two realms; first with respect to the theoretical standard, and second with respect to the epitaxially grown graphene on SiC. Indeed, selection of this collection of substrates offers a quantitative window into further examining the effects of processing by comparing epitaxially grown graphene on SiC with CVD grown graphene that is later transferred onto SiC substrates. It is worth emphasizing that multiple layer graphene is an additional variable here, known to enhance conductivity,[33] where a multiplicity of stacking geometries enables tailoring of band structures.[34] In this scenario, initially nucleated deformation might propagate throughout the graphene stack or further relax depending on subsequent substrate interactions.

Sample fabrication

Graphene monolayers were grown on Copper foil by chemical vapor deposition (CVD) method in a tube furnace (OTF-1200x-S^{TM}, MTI Corp, CA) equipped with a scroll vacuum pump.[10, 35] The Cu substrate was purchased by Lester Metals llc, Avalon Lake, Ohio, with a 99.99% purity

to yield oxygen-free Cu foil with 0.0005% O content, consisting of multidomains of ~10 μm diameter sized grain boundaries. X-ray diffraction (XRD) measurements of the Cu foil shows <200> is the preferred orientation of the polycrystalline grains, with a weaker <111> contribution, as shown in Figure S1 in the Supporting Information (SI).

Whilst the Cu foil was heated up to 1000 °C, hydrogen gas was injected at 125 mTorr for 30 min, followed by injection of methane gas at 1.25 Torr for a further 30 min; the furnace was then cooled down to room temperature while the flow of hydrogen and methane remained. In preparation for graphene transfer, SiC substrates were solvent-cleaned through 15-minute submersion steps trough an Acetone, Methanol and Isopropyl alcohol sequence. The cleaning and transfer procedures took place in a class 10000 cleanroom, with the cleaned substrates being used immediately.

Transfer onto SiC substrates were achieved using a thermal release tape (Nitto Americas Inc., CA). The tape was placed over the graphene-coated Cu foil. A round metal bar was gently rolled over the thermal release tape to secure the adhesion. Oxygen plasma (35mW/cm^2) was applied on the exposed graphene-side of the Cu foil for 5 min to remove extra graphene and expedite the following chemical Cu etching process. The ensemble was then etched in 100 mg/mL $(NH_4)_2S_2O_8$ solution for 2 hr, rinsed with deionized water, and dried with dry N_2. Upon drying, the graphene/thermal tape ensemble was layered onto SiC, as seen on the Etch/Rinse step in Figure 1a. The SiC/graphene/thermal release tape ensemble was then heated at 125 °C to release single monolayer graphene onto the substrate. Toluene washing was applied to the transferred graphene to remove adhesive residues from the tape. This single layer graphene transfer process was sequentially applied four times to prepare four monolayers graphene onto both Si- and C-terminated SiC substrates. Figure 1(a) summarizes the fabrication process described here.

Following the above procedure, graphene single monolayer/four monolayers were transferred onto both Si- and C-terminated SiC. Indeed, our previous work on quartz crystal microbalance (QCM) based quantitative measurements for 1 layer to 4-layer thermal released tape transferred CVD graphene confirms that the repetitive graphene transfer used in this work is a reliable process for single to multilayer graphene on a hard metal/quartz substrate. Kim showed that the linear fit of 89.1 ng/cm^2 transferred-graphene was in close proximity to a theoretical single layer graphene aerial weight of 76.1 ng/cm^2.[36]

Following the same procedure, graphene was also transferred to a SiN transmission electron microscopy grid towards examination by Helium Ion Microscopy. In addition, epitaxially-grown single graphene monolayer on Si-terminated SiC was also fabricated for comparison.

Epitaxial graphene was grown on commercial nominally on-axis oriented 6H–SiC (0001) (SiCrystal AG, Germany). Prior to epitaxy, surface polishing damage was removed through etching in hydrogen for 15 min. at 1 bar and 1550 °C. Epitaxial growth was performed in a vertical cold-wall reactor with a double-walled, water-cooled quartz tube and a graphite susceptor in a slow flow of argon (purity 5.0). Heating and cooling rates were 2–3 °C per second. Typical annealing time was 15 min.

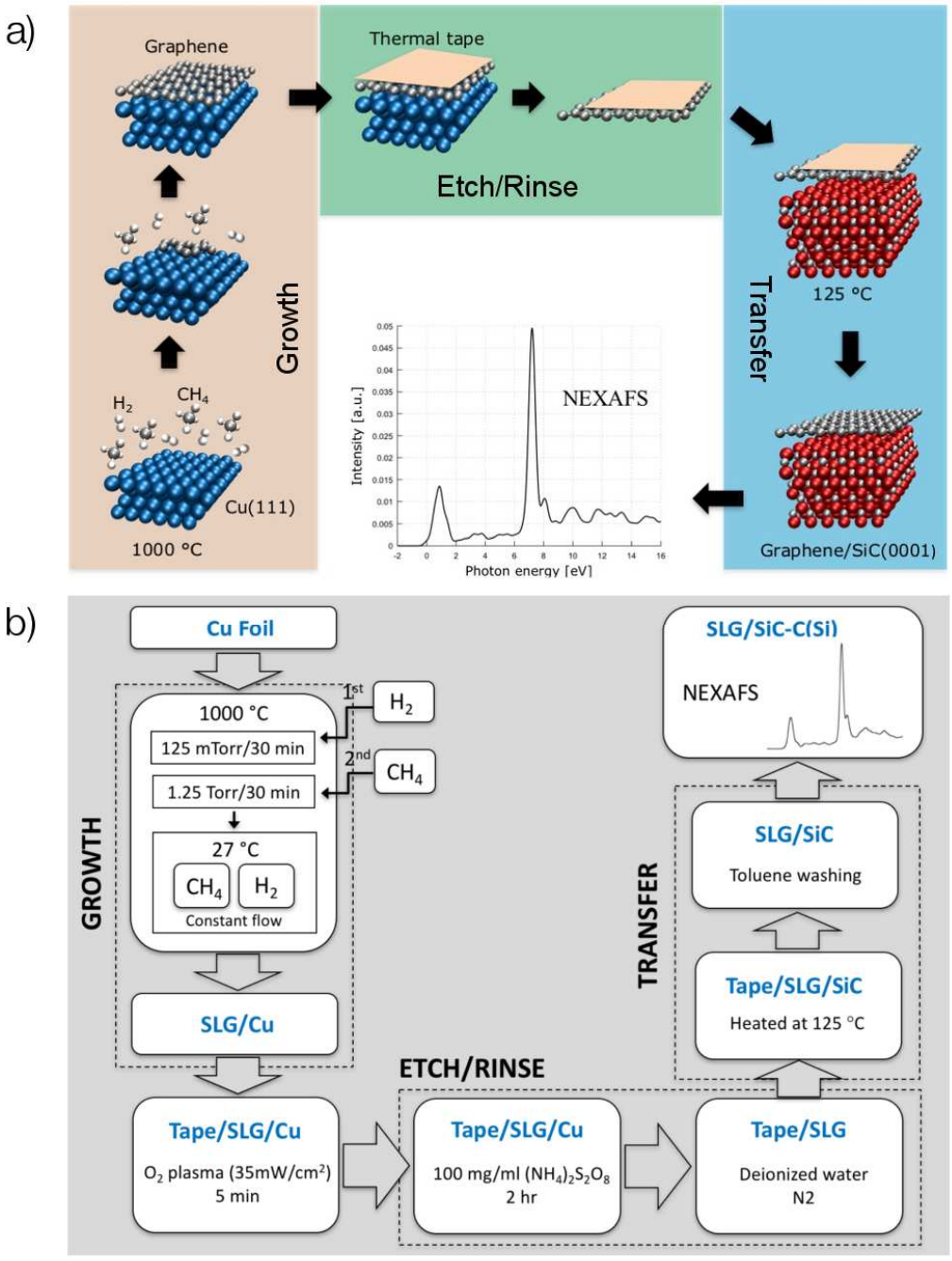

Figure 1. (a) Schematic showing fabrication, transferring and subsequent NEXAFS analysis of 1 transferred graphene layer. (b) Growth-transfer process details of graphene onto silicon-terminated SiC substrate. The process was later repeated 4 times to yield a 4-layer transferred ensemble.

Characterization

Experimental Carbon K-edge NEXAFS spectra were acquired at Beamline U7A (NSLS-I BNL) equipped with a LARIAT I detector (NSLS, Synchrotron Research Inc.) at the National Synchrotron Light Source, Brookhaven National Laboratory at 85° incidence of X-rays relative to the plane of the sample in partial electron yield (PEY) mode, with energy resolutions of 0.1 or 0.2 eV. The polarization is 85% in the horizontal direction. NEXAFS measurements were performed in partial electron yield (PEY) mode. Depth sensitivity in PEY NEXAFS is dependent on the kinetic energies of the collected electrons, but can be tuned in part by the application of a grid bias prior to the detector.[37, 38] The grid acts as a high-pass filter, rejecting elastically-scattered electrons with lower energies which are likely to have been emitted from deeper within the sample. C K-edge measurements were performed with a grid bias of -225 V. A lower limit for the depth sensitivity can be taken as the inelastic mean free path of the C KLL signal (E_K=263 eV), which will comprise a significant portion of the detected signal with this grid bias; this is estimated to be 0.7 nm assuming a graphene density of 2.3 g/cm^3.[37] Spectra normalization was performed with the LDF software (Synchrotron Research Inc.) and the scanned areas were 5 mm × 3 mm in size.

The systems reported in this paper are CVD SLG grown on Copper, and CVD graphene (single layer and four layers) grown on Copper transferred to both Si- and C-terminated SiC. Epitaxially grown graphene on SiC was also measured for comparison. Figure 1 shows the process from fabrication to transferred graphene onto a target substrate.

For Helium Ion Microscopy characterization, untreated CVD-grown graphene was transferred to a SiN grid and imaged in an ORION Plus He-IM Zeiss at 30kV and the assistance of a flood gun was not necessary to prevent surface charging.

Geometry relaxation and Band structure calculation

Structural relaxations were carried out using plane-wave density functional theory (DFT) implemented in Quantum Espresso within the pseudopotential approximation.[39, 40] We employed ultrasoft pseudopotentials, energy cutoffs of 30 Ry for plane wave basis set and 320 Ry for charge density, k-sampling grid in the Monkhorst-Pack scheme of 30×30×1 and vacuum of ~15 Å along the Z-axis. Total energy and electronic self-consistency criteria were set to 10^{-6} Ry and 10^{-8} Ry. Atomic forces at equilibrium position were converged below 0.01 eV/Å. All relaxations were modelled under the general-gradient approximation (GGA) with the Perdue-Burke-Ernzerhof (PBE) exchange-correlation functional.[41, 42] The workflow is shown in Figure 2(a).

A single layer of graphene conformed onto copper substrate along the (111) surface orientation (SLG/Cu) and free-standing graphene (SLG) samples of 2.42 Å, 2.47 Å and 2.51 Å lattice parameters were modelled. SLG was simulated considering a unit cell of 2 C atoms whereas for SLG/Cu the unit cell contains 4 Cu atoms, one per each layer, and 2 C atoms for the SLG, as well as, considered the most stable configuration *top-fcc*. Lattice constants of Cu substrates has been adapted to graphene accordingly, as depicted in Figure 2(b).[43, 44] Interface distance of 3.25 Å, accurately calculated by Olsen *et. al*. under the random phase approximation (RPA) to consider interface chemical bonding and van der Waals interactions, has been taken for all SLG/Cu systems.[24, 45] Ground state band structures were performed by sampling the Brillouin Zone with 200×200×1, where convergence of Fermi energy is achieved within the self-consistent field calculations of ± 0.01 eV. High symmetry k-points (M and K) were explicitly included.

Graphene ripple was relaxed under same criteria of SLG and SLG/Cu except that k-sampling grid in the Monkhorst-Pack scheme of 10×10×1 and equilibrium atomic force of 0.02 eV/Å were applied. The supercell contains 200 C atoms.

NEXAFS simulation

To simulate NEXAFS, supercells assembled by 7 replications of unit cell along X and Y axis has been employed. This supercell's size provides a suitable distance between absorbing atoms to avoid interaction between them due to the periodic boundary conditions. Such supercell size contains 98C atoms for each SLG and 294 atoms (98 C and 196 Cu atoms) for SLG/Cu. *Ab-initio* NEXAFS spectroscopy calculations at C K-edge were modelled in the framework of the excited electron and core-hole (XCH) approximation at 55° of incidence of an X-ray beam to enhance π* and σ* resonances; which was implemented in the in-house code Shirley by one of the authors.[46] In order to simulate the excitation of the carbon atom due to the X-ray, one electron from the 1s level of the carbon pseudopotential has been removed. One carbon atom from the supercell has been used to calculate the unoccupied states under the pseudopotential approximation that includes the core-hole interactions. XCH-NEXAFS uses the PBE form for the exchange–correlation potential within GGA approximation. A simplified scheme of the procedure to simulate NEXAFS is shown in Figure 2(a). A final alignment with experiment has been carried out through the electronic transition π* C=C of 285 eV for every NEXAFS spectra simulated.

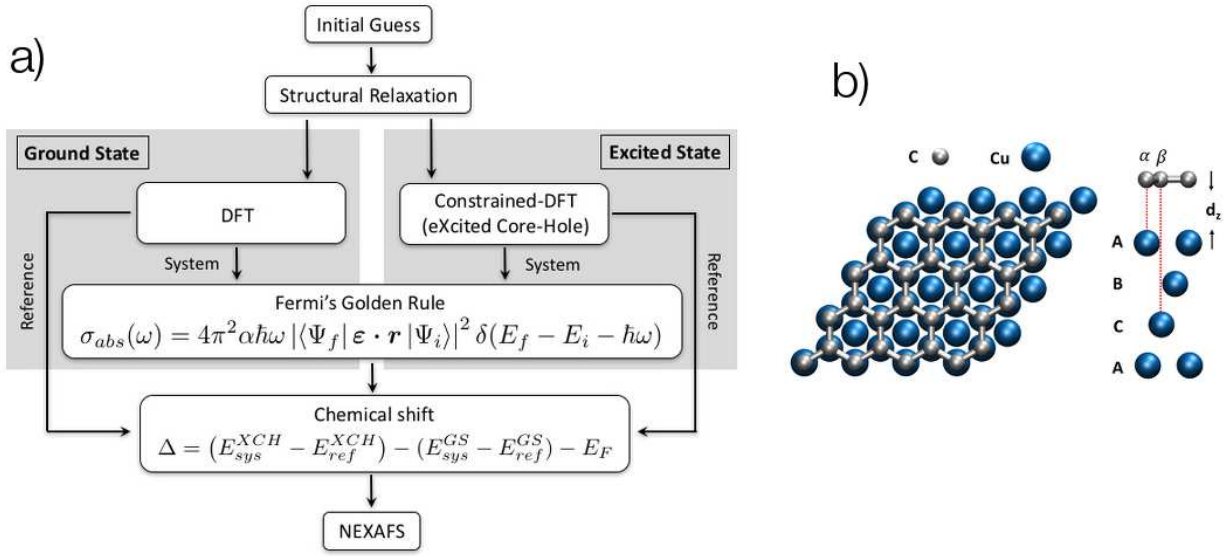

Figure 2. Schematics describing first-principles NEXAFS calculations of SLG and SLG/Cu, where (a) the procedure to calculate NEXAFS from first-principles details the calculation of chemical shift embedded in the Shirley code. This chemical shift is the result of variation of excited total energy of the system (E_{sys}^{XCH}) respect to isolated excited atom (E_{ref}^{XCH}) and ground total energy of the system (E_{sys}^{GS}) respect to isolated atom at ground state (E_{ref}^{GS}), then it is set to the Fermi energy of the system. For instance, the chemical shift calculated for SLG/Cu of 2.51 Å with the Shirley code showed a value of -1.87615 eV (Chemical shift = [-13445.55631458 - (-18.71081349)] – [-13437.59127593 - (-10.71888784)] * 13.6 eV - 2.24196267040978 eV = -1.87615 eV) (b) Most stable top-fcc atomic configuration of SLG/Cu represented by four atomic layers of Cu where the two carbon atoms (α and β) in SLG unit cell cover Cu atoms in layers A and C.

Results and Discussion

Graphene films were etched from the Cu substrates and transferred to SiC wafers, as shown in Figure 1(a), to be analyzed through both experimental and theoretical NEXAFS spectroscopy. The substrates of choice were Si and C- terminated SiC so that the resulting single and multiple layer stacks on SiC could we compared to the experimental standard epitaxial SLG/SiC. Transfer engineering allows for multiple layer stacking, with the possibility of favoring device mobility so that 4LG/SiC samples on both terminations were assembled and also examined by NEXAFS spectroscopy. Indeed, multiple layer graphene is an additional variable here, known to enhance conductivity,[33] where a multiplicity of stacking geometries enables tailoring of band structures, inclusive of band-gap opening.[34] In this scenario, initially nucleated deformations might propagate throughout the graphene stack or further relax depending on subjacent substrate interactions.

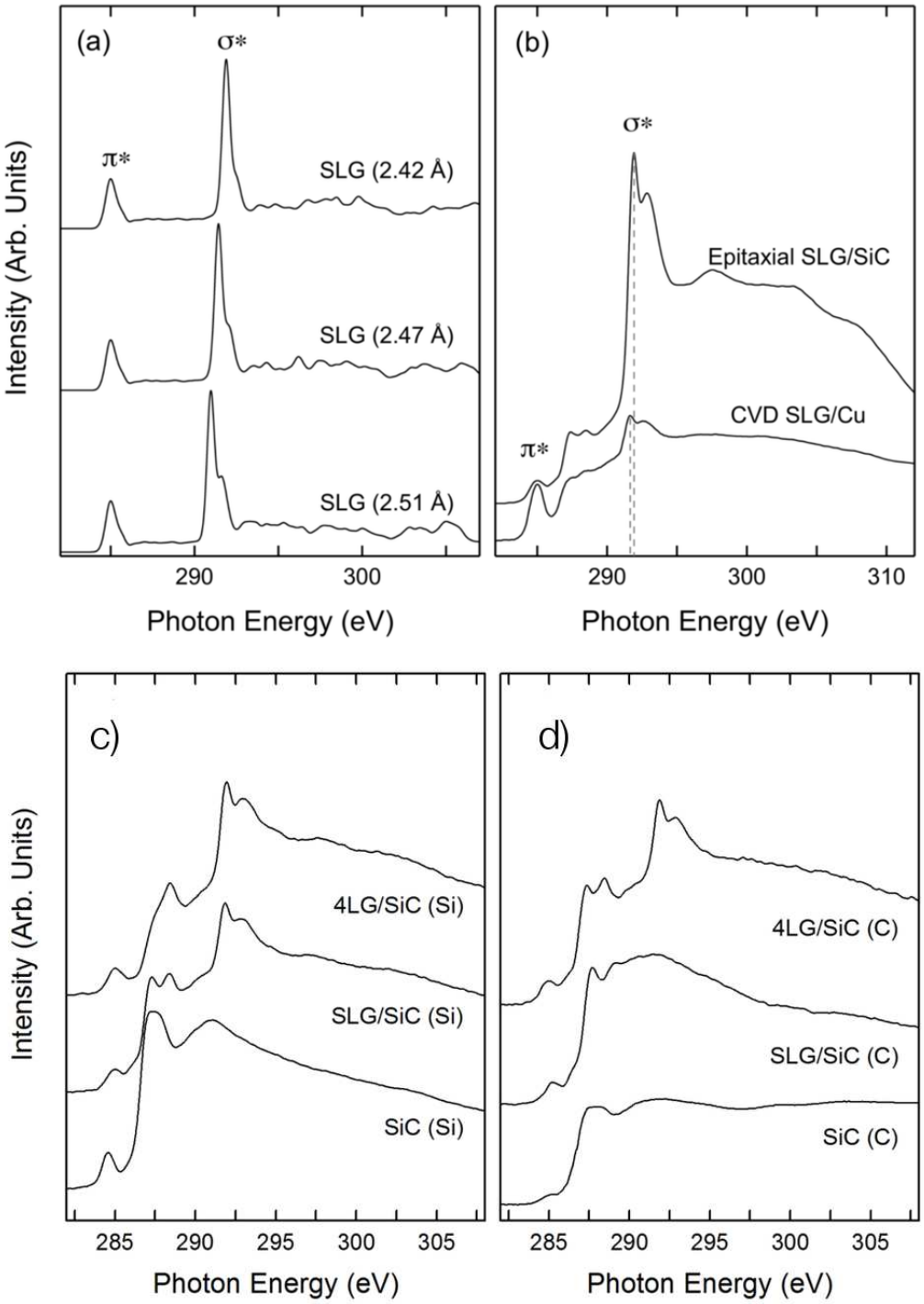

Figure 3. (a) Calculated C K-edge NEXAFS spectra of SLG. Position of σ* resonance is a function of graphene lattice parameter, or bond length. (b) Experimental C K-edge NEXAFS of epitaxially grown graphene on SiC and chemical vapor deposited graphene on copper result in

different carbon–carbon bond lengths, evidenced by different σ* resonance energy positions. Experimental C K-edge NEXAFS spectra of single-layer graphene and four graphene layers transferred onto Silicon-terminated (d) and Carbon-terminated (d) SiC substrate.

As described in methodology, both theoretical (Figure 3(a)) and experimental spectra (Figure 3(b-d)) of graphene are considered in this discussion. In particular, theoretical spectra of graphene with different lattice parameters (Figure 3(a)) will be used as a theoretical standard in this discussion. Similarly, spectra of epitaxial SLG/SiC and CVD/Cu (Figure 3b) will be considered an experimental standard. Spectral signatures from both standards will be compared against spectral signatures from processed (i.e. transferred) graphene and from SIC substrates in both Si and C terminations (Figure 3(c-d)).

Presence of π* C=C intensities at 285 eV on SiC substrates (Figure 3(b-d)) show signs of contamination, resulting from exposure of SiC substrates to enviromnments outside cleanroom settings, prior to synchrotron experiments. Experimental spectra of transferred SLG in all scans in Figure 3(c-d) is dominated by π* C=C intensities at 285 eV, σ* C-H at 287 eV, π* C=O at 288 eV and σ* C-C at 292 eV as expected.[18] The different properties of graphene grown on Si and C terminations of SiC have been well documented,[12] and these results suggest that the SiC termination also has an effect on NEXAFS spectra of transferred CVD-grown graphene. In particular, while the spectrum of SLG/SiC(Si) in Figure 3(c) is dominated by graphene, the distinctive sharp σ* resonance of graphene is not observed for SLG/SiC(C) in Figure 3(d). Instead, a broad σ* resonance is recorded, which is attributed to the convolution of σ* C-C and σ* Si-C signals from the substrate (Figure 3(d)). Indeed, measurements from SLG/SiC-C do not resemble typical graphene spectra (Figure 3(d)). These findings indicate that the spectra collected from SLG/SiC-C is dominated by the substrate. Along those lines, experimental and

theoretical spectra of SiC in both 3C and 6H polytypes have been examined by Pedio and coworkers and show comparable signals as those shown here,[47] with higher texture in the 287, 288 eV and 292 eV regions for 6H-SiC than for 3C-SiC, as shown in Figure 3).

The spectrum from SLG/SiC-Si owes its clear predominance of the graphene signal to the Si atomic layer residing between carbon in the substrate and graphene,[9] which suppresses Auger emissions from the substrate. Upon four monolayers transfer, the substrate termination produces little effect in NEXAFS spectra, other than increased intensities of oxygenated states. Decreased intensities at 287 eV in 4LG/SiC(Si) suggests that C-H impurities could be mostly in the substrate. Conversely, π^* C=O signal ~ 288 eV has a decresased intensity in the substrate and increases with graphene in both terminations, suggesting carboxylic impurities are being generated on the graphitic structure througout chemical processing.[48]

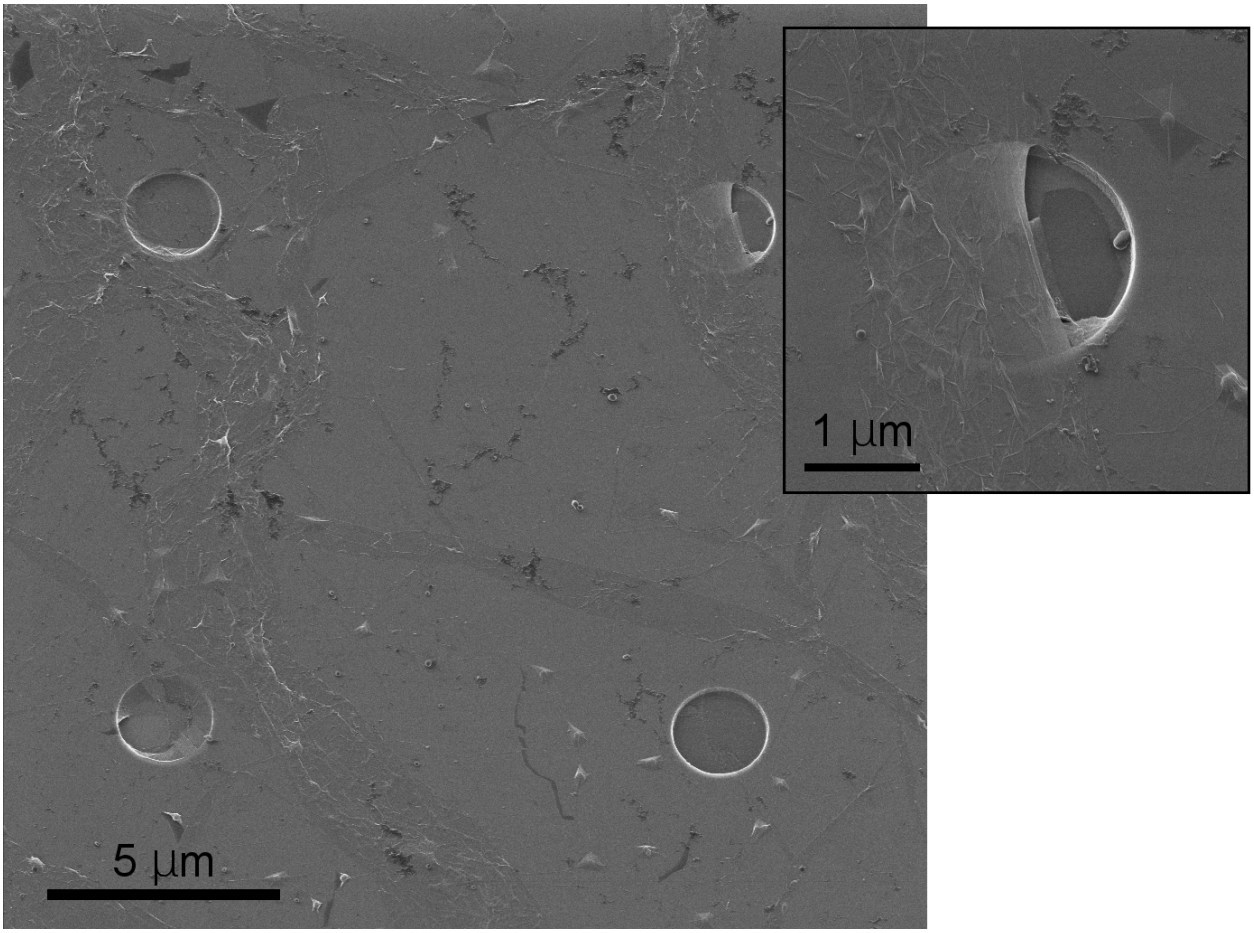

Figure 4. He Ion Microscopy (He-IM) of CVD-grown graphene grown on Cu and later transferred to a SiN TEM grid. This technique conveniently emphasizes characteristic ripples of ~50 nm width that are visible throughout the sample.

From a morphological perspective, the extent of large out of plane mechanical deformations can be conveniently described through He Ion Microscopy (He-IM).[49] He-IM images of CVD-grown graphene on Cu transferred to a SiN TEM grid show extensive regions of high corrugation, even on the freestanding portions, with features up to 50 nm wide, combined with flat areas, as seen in Figure 4. The scan width in this micrograph is 15×15 μm^2, whereas scanned regions at the NEXAFS scans were 5×3 mm^2. He-IM imaging of soft matter systems is well known to reproduce topographic features with high fidelity, which indicates the observed

corrugation was not originated by electron beam heating.[50] In addition, absence of coating layers to prevent charging also guarantee high fidelity of graphene rippling effects, which are the result from growth and transfer to any given substrate, albeit with varying widths and heights. Widths from tens to hundreds of nanometers as well as heights of up to 6 nm have been recorded by AFM upon transfer.[16] In addition to the obvious out of plane features, in plane effects will also result from growth and processing, whose morphological description requires of high resolution TEM or STM approaches that will, nonetheless, only provide a description at a very local level.[9]

With the purpose of solving this sensitivity/length scale conundrum, the present approach combines the experimental NEXAFS data above with theoretical spectra to analyze mechanical deformation through lattice parameter variation at wafer scales; paving the way to industrial application.

On those lines, three theoretical standards were constructed with free standing graphene of lattice parameters reported in the literature 2.42 Å,[23] and 2.47 Å,[24] as well as 2.51 Å for completion. These structures were relaxed through first principle procedures, as highlighted in the methods section and briefly introduced in Figure 2(a) and the flow of the experimental/theoretical sequence is shown in Figure 1(b). It is worth highlighting that these calculations resemble earlier ones by some of the authors, now with a smaller 7×7 supercell for computational economy that did not produce undesirable edge effects on the spectra and showed consistent fingerprints.

The resulting NEXAFS spectra through the excited core hole approximation yielded by the Shirley code, as described in the methods section, are shown in Figure 2(a) and constitute a set of theoretical standards against which experimental data will be compared. On a first level comparison, experimental NEXAFS of epitaxially grown SLG on Cu through CVD methods and

on SiC through Si sublimation (i.e. experimental standards reported here) have also been measured, as shown in Figure 3(a). Since substrate effects need to be addressed, calculations also were performed on graphene grown on Cu, (SLG/Cu); which will be discussed in the next section. These calculations feature the reportedly most stable top fcc configuration, as described in Figure 2(b),[43, 44] and an interface distance d_z of 3.25 Å, as reported by Banerjee et al, to adequately describe the van der Waals interaction between Cu and SLG.[24]

Both calculated (projected to 55°) and experimental (acquired at 85°) NEXAFS spectra of graphene standards feature typical 1s → π* C=C and 1s → σ* C-C electronic transitions at ~285 and 291 eV respectively (Figure 3(a-b)).[18, 23] In addition, experimental spectra show peaks between 287 and 288 eV attributed to σ* C-H and π* C=O impurity states, similar to those in Figure 3(c-d). At this time, a discussion is needed per the depth sensitivity of the reported signals. As mentioned earlier, both experimental and theoretical spectra have confirmed surface termination-sensitivity in NEXAFS studies on SiC.[47] In addition, polarization and detector bias variations have yielded descriptions of the graphene/susbtrate interactions.[9]

The assignment of C-C σ* intensities and correlation with bond length has been a controversial topic of research in the NEXAFS literature pertaining to molecules where conjugation and localization effects have been thoroughly discussed by Piancastelli and Stohr.[51,52] Historically, the bond length correlation model sought to establish an empirical relationship between bond lengths and the energy position as well as the lineshape of a σ* resonance. While the model works reasonably well for simple diatomic molecules, it is of limited utility in systems with more delocalized sigma bonding such as benzene. In recent work, the core excitonic nature of C-C σ* states in graphene have been confirmed,[53] building upon Ågren's

theoretical and Brühwiler's experimental work, which has also confirmed the core excitonic character of the ~292 eV intensity associated to sp^2 graphite.[54, 55] Interestingly, density functional theory calculations suggest a clear empirical correlation between the peak position of σ* resonances and bond lengths of graphene, which likely derives from the relatively localized excitonic nature of the resonances. However, this assumes entirely uniform strain with retention of conjugation. While the limits of this correlation have not been explored, the calculated empirical correlation provides a valuable means of assessing substrate-induced strain effects. First, on the interpretation realm, we have calculated the effects of substrate charge transfer (Figure S2) and substrate screening to graphene NEXAFS spectra (Figure S3), to which σ* shifts can also be attributed. We have found both these effects to be small for Cu substrates. This discussion has been fully detailed in the SI and will be further developed in the next section. Second, on the computational realm, we have confirmed that in-plane strained graphene leads to a shift of the σ* resonances exclusively, Figure 3(a-b), and no hybridization with the π* C=C signals in the graphitic lattice is possible. Similarly, adjacent atoms in an out of plane deformation, i.e. along a ripple, will also present shifted σ* resonances (see upcoming section "Interpretation of σ* shifts as they correlate to strain and lattice parameter"); indicative of lattice parameter variation, since hybridization with adjacent π* C=C signals is not viable. The density functional theory calculations thus provide a practical measure of strain within the samples likely as a result of the highly excitonic nature of σ* resonances.

Lattice parameter calculations

Shifts in σ* energy positions are clearly observed in experimental spectra of epitaxial SLG/SiC and CVD SLG/Cu (Figure 3(a-b)). These scans produced σ* resonances at 291.8 and 291.3 eV

respectively, suggesting a smaller lattice parameter in CVD SLG/Cu than in SLG/SiC. Further, transferred SLG onto SiC substrates produced σ* energy positions shifted by different amounts at 291.8 eV for SLG/SiC(Si), and 291.9 eV for both 4LG/SiC(Si) and 4LG/SiC(C). Growth method, substrate, and processing differ in the experimental samples discussed here. However, for the calculated spectra the only variable is the bond length, yet spectra still produced σ* shifts with varying bond lengths. Hence, taking into account the discussion in the prior section, we are attributing differences in C–C bond lengths as reflected in experimental NEXAFS to effects from growth, substrate, and processing. Indeed, of the three substrate-related factors discussed in the prior section, substrate shielding effects can be bypassed by monitoring E(σ*) – E(π*) rather than absolute σ* energies in the prediction of bond lengths for Cu-derived systems, which follows. As a consequence, and given that charge transfer is below the experimental resolution, all σ* energy positions from Cu-derived graphene (both grown and transferred) in this discussion reflect lattice parameter exclusively. In this calculation, epitaxial SLG/SiC is also tentatively included. However, this system will be discussed further below, due to the undocumented effects of substrate shielding.

In the time-independent density functional theory calculations, graphene with various lattice constants were used as theoretical standards to fit a linear relationship between σ* resonance energy E(σ*) – E (π*) and bond length R of the form:

$$E(\sigma^*)\text{-}E(\pi^*) = aR + b \qquad (1)$$

In this approach, we have calculated theoretical standards (SLG and SLG/Cu) with lattice constants 2.42, 2.47, and 2.51 Å, which has the underlying assumption of uniform strain. A theoretical study of freestanding SLG, addressed band structure engineering by strain through first principles calculations,[56] and found that the characteristic band structure from graphene was

lost for those values of lattice constants above 3.209 Å. These findings justify the choice of lattice parameters of theoretical SLG standards; whose band structures (both as free standing and as SLG/Cu) have the expected graphitic components. In fact, we have taken an experimental value from CVD SLG/Cu from the literature with lattice constant of 2.46 Å, which is close to the typically used reference of *graphite,* with lattice constant 2.461 Å.[31, 56]

In order to follow the rationale above and measure exclusively σ* shifts irrespectively of substrate effects, E(σ*) – E(π*) as given in Eq. (1) was used to predict the bond lengths of experimental samples as shown in Figure 5, and in agreement with discussion in the prior section. Notably, we have plotted E(σ*) – E(π*) versus lattice parameters from the theoretical standards associated to SLG and to SLG/Cu, as seen in Figure 5, both linear fits showing a slight difference in fitting parameters, as highlighted in the caption. Indeed, as it was shown in Figure 5, charge transfer effects had a subtle effect on σ* energy positions, whose associated shifts were on the order of 0.01 eV, much below the energy resolution limit in the present setup. For consistency, we have used the regression associated to SLG/Cu to predict the bond lengths of the experimental as-grown and of transferred samples, for which only the E(σ*) – E(π*) is known through experimental NEXAFS.

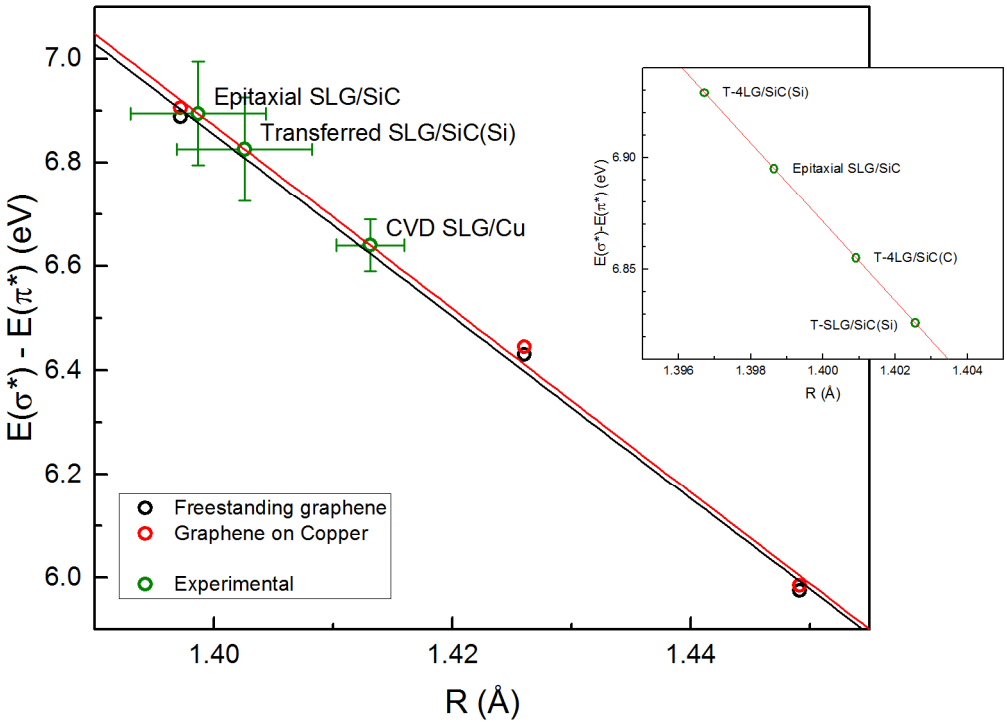

Figure 5. The carbon–carbon bond lengths (R) for the various graphene systems display the predicted linear correlation with the σ* resonance energy position, as discussed in the text. Linear fits with equation (1) from the text yielded the fitting parameters a = -17.5 and b = 31.6 for freestanding graphene, and a= -17.6 and b= 31.6 for SLG/Cu. For both freestanding SLG and SLG/Cu, the correlation coefficients are close to unity, indicating a reasonable empirical description of the relationship between R and σ* resonance energy position. Data points represented by black and red circles have been theory-derived to yield a linear fit on which experimental σ* resonance energy positions are placed atop to deduce values of R. Green circles represent the deduced values of R. The inset shows the same regression magnified in the 6.80-6.95 eV and 1.3905-1.404 Å where data from transferred and epitaxial graphene lie.

Figure 5 shows the bond length predictions of CVD SLG/Cu and of epitaxially-grown SLG/SiC (Figure 3(b)). In fact, the predictions were derived from the regression tendered from the calculated SLG/Cu. The experimental error for predicted bond lengths is calculated as the energy resolution (0.05 and 0.1 eV for beamlines U12 and U7 respectively) divided by fitting parameter a in Equation 1. The inset in Figure 5 shows the bond length predictions for the transferred systems.

The prior section established that charge transfer in graphene grown on SiC is small, and therefore not affecting σ* resonance energy positions. An additional clarification is needed here in the context of SiC, not as growth but as transfer substrate. In this scenario, it is worth highlighting that those SLG that have been transferred will likely engage in Van der Waals interaction with the subjacent SiC substrates. Since the transfer is conducted at temperatures much below those typical in growth; it is expected that those van der Waals interactions will be weak, therefore yielding no charge exchange or any other substrate artifact and hence, producing no spectral signature and justifying the predictions in SiC transferred systems.

With all, values of bond lengths of CVD SLG/Cu, Epitaxial SLG/SiC and transferred SLG to SiC on both terminations were predicted through the regressions in Figure 5 and plotted in Table 1 along with calculated strain values with respect to a CVD grown experimental standard found in the literature with lattice parameter 2.46 Å,[31] which is a similar value to graphite, often used in the literature as a comparative standard in the calculation of strains**.**

Strain was calculated with the following equation:

$$\text{Strain} = \left[\frac{R_{predicted} - R_{reference}}{R_{reference}}\right] \times 100\%$$

Where R is bond length and the bond legth used for reference (1.42 Å), which is indeed a value from the literature that was derived from Low Energy Electron Diffraction measurements on CVD-grown graphene on Cu substrate as reported by Avila. [1]

In this study, we have used SiC as transferred substrates aimed at comparing the resulting ensembles with epitaxial SLG/SiC as well as SLG-Cu as experimental references. It is clear from Figure 3(b) that the growth substrate influences the carbon–carbon bond length. We note that predicted C–C bond lengths of all experimental systems, shown in Table 1, are lower than the typically cited length of 1.42 Å by less than 2%.[20] In fact, Gui et al estimated that under small strain (less than 2%) the Poisson ratios in the two directions take the same values, indicating that graphene is isotropic (deformation along X and Y axis take same values).[56] Under even smaller strain (less than 1.5%), the Poisson ratios were constant (0.1732). According to this discussion, values in Table 1 (below 2%) suggest that transferred SLG are all under compressive isotropic strain, and the predicted values are within the available experimental findings in the literature.

Table 1. Predicted carbon-carbon bond lengths for all studied graphene systems. R(A) correspond to values of bond length of the standards, which are free standing graphene and graphene on Cu. These are theoretical samples, and R(A) is the bond length value by design on free standing graphene and the value of bond length for Graphene on Cu at the interface distance reported by Olson. Predicted R(A) are values of bond lengths that have been estimated over experimental samples with the assistance of theoretical standards, where a correlation between bond length and Sigma emission energy was established.

System	E(σ*)-E(π*) (eV)	R (Å)	Predicted R (Å)	Strain (%)
SLG (2.46 Å)*	---	1.42	---	---
SLG (2.42 Å)[a]	6.888	1.397	---	-1.62
SLG (2.47 Å)[a]	6.430	1.426	---	0.42
SLG (2.51 Å)[a]	5.975	1.449	---	2.04
SLG/Cu (2.42 Å)[b]	6.906	1.397	---	-1.62
SLG/Cu (2.47 Å)[b]	6.446	1.426	---	0.42
SLG/Cu (2.51 Å)[b]	5.985	1.449	---	2.04
CVD SLG/Cu	6.64± 0.05	---	1.413 ± 0.003	-0.49
T-SLG/SiC(Si)	6.8± 0.1	---	1.403± 0.006	-1.17
T-4SLG/SiC(Si)	6.9± 0.1	---	1.398± 0.006	-1.57
T-4SLG/SiC(C)	6.8± 0.1	---	1.403± 0.006	-1.17
Epitaxial SLG/SiC	6.9± 0.1	---	1.398± 0.006	-1.57

[a] Calculated NEXAFS spectra where the graphene lattice constant is given in parentheses.

[b] Spectra used to fit Equation 1.

* Ref (Avila, et. al.)[31]

Table 1 indicates that Epitaxial SLG/SiC, for instance, has a strain of -1.57%; suggesting an overestimation, since it is commonly thought that the maximum strain possible would be on the order of 1%.[9, 57] Albeit, we are using three theoretical graphene systems to calibrate a line through which we predict bond lengths of real systems which are far from pristine graphene, as shown in the HeIM image in Figure 4. This will be addressed further in the section below.

Interpretation of σ* shifts as they correlate to strain and lattice parameter

At this time, it is unclear how individual morphologies throughout the scanned regions are contributing to a strain variation. Indeed, the dynamics of how their spectroscopic signatures are combined to produce a certain σ* position which yields a certain amount of strain have not yet been discussed. Incidentally, it is worth highlighting that in unsupported graphene (equivalently, graphene that is not experimenting effects from subjacent substrates like the transferred systems), by assuming theoretical SLG (2.47 Å) as standard, we find SLG (2.42 Å) is compressed by little under 3%. Even under this large strain, graphene properties—both electronic and crystallographic—remain unchanged according to the band structure as shown in Figure S2 (b).

It should also be noted that while the theoretical models are molecularly homogenous, where every bond is uniformly strained by the same amount. However, experimental spectra average through morphologies that include multiple local inhomogeneities such as localized strain and rippling, as seen in Figure 4. With the purpose of analyzing at the atomic level, a rippled morphology, showing strained bonds throughout, has been modeled.

More specifically, in a rippled region, such as that described in Figure 6, we have calculated spectra associated to atoms along the ripple. In this scheme, the associated σ* resonances were also plotted (Figure 6 right) to reveal energy shifts in the σ* resonance associated with individual strained bond lengths. The single strain value predicted for an experimental system is the result of strain homogeneities throughout the scanned region. The variation of σ* energies for atoms 1 and 10 has been highlighted; showing the sensitivity of this technique to capture variations at the atomic scale that will be further averaged. In fact, we have verified that the average spectra along

the rippled region provides a σ* energy position that is the resulting average of the individual shifts from each atom along the ripple.

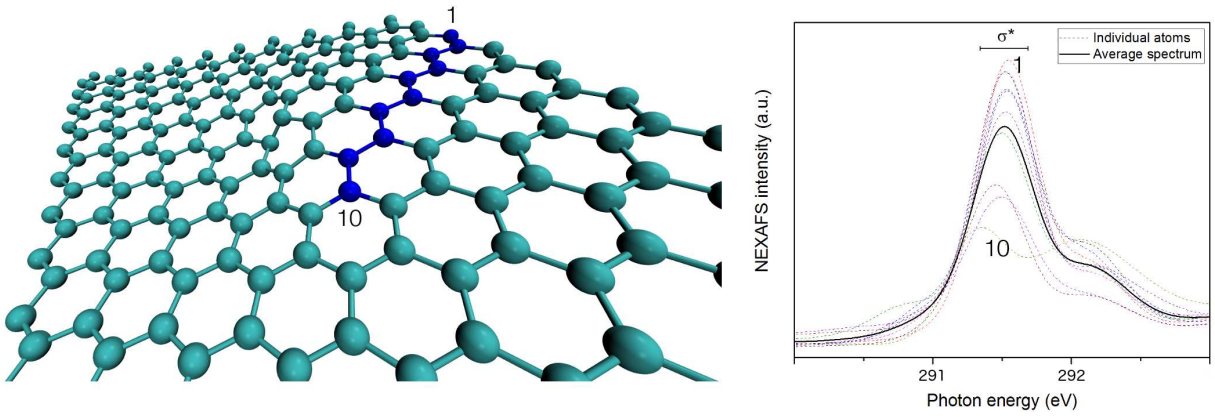

Figure 6. Theoretical NEXAFS calculations for atoms along a graphene ripple. Individual atoms produce σ* resonances at various energies, indicating different bond lengths.

These results suggest that every morphology is going to contribute to the measured integrated σ*, allowing the identification of an unevenly deformed real system with a certain value of strain to an equivalent homogeneously strained system. Both would indeed yield the same integrated spectra. It is important to remember that σ* shifts register not only in plane strain, but out of plane strain as well. Albeit, high curvature in large corrugations might not be registered due to transition prohibition, or, geometrically, due to the orthogonality of beam polarization and vector associated with the σ* orbitals.[19] However, most morphologies will be captured by this technique.

It is important to emphasize that this technique provides a clear description of the value of averaged spectra over large areas. The large areas are inclusive of wafer size regions- where the molecular detail of individual atoms is preserved and averaged out with the collective. These NEXAFS-specific capabilities are further emphasized through the value brought forward by large area hyperspectral NEXAFS. Indeed, with a dynamic range between 40 μm to the tens of

mms, this analysis can be deployed in specific regions of interest as well as to the overall wafer; opening the possibility of thorough strain metrics.

Given the interest on the increased transport properties resulting from stacked configurations upon multiple transfers,[33] as mentioned previously, it is worth highlighting this methodology allows for the characterization both at wafer and micron levels (due to the advent of hyperspectral spectroscopy) of transferred graphene to substrates of technological relevance, beyond native substrates.

Following transfer of a single layer to SiC(Si), the bond length of CVD SLG/Cu decreases to 1.403 Å. On transfer of subsequent layers the bond length is further decreased. However, prior to providing an interpretation on the specifics behind transferred systems, a comparative discussion is needed on the experimental standards CVD SLG/Cu and epitaxial SLG/SiC.

Bertran et al. demonstrated how fine control over experimental variables such as H_2 flow could have a large impact over strain on CVD SLG/Cu.[58] Indeed, by measuring Raman shifts of the 2D phonon mode compared to that of unstrained pristine graphene, compressive strain could be lowered from 0.2% to 0.026%. Further, by combining Raman spectroscopy with molecular dynamics simulations, He et al. confirmed an average compressive strain of 0.5% for CVD SLG/Cu, which is the resulting average of local C-C bond lengths being deformed in the amounts of 0.009-0.005 Å, which yield strains between 0.3% and 0.6%.[59] These results suggest that the predicted strain in CVD SLG/Cu (-0.49%) in Table 1 falls within the expected range.

Discussion of the experimental standard SLG/SiC is less straightforward. Indeed, growth of epitaxial graphene has been recently reviewed; biaxial strain first arises from epitaxial stress during graphene growth on a substrate, and is energetically costly.[9] In fact, strain in excess 1% has been quoted as prohibitive, since it cannot even be achieved in the graphene–metal

systems. In the present scenario, strain predicted in SLG/SiC is compressive by 1.57%, which is not consistent with Tetlow's parameters. In addition, engaging in the calculation of band structure and NEXAFS spectrum of epitaxial SLG/SiC is computationally expensive. As mentioned earlier, Coletti et al have measured the Dirac point energy on a SLG/SiC ensemble to be on the order of 0.42 eV, comparable to that observed in SLG/Cu, which produced little impact on the σ* shift.[60] These results led to the conclusion that charge transfer in SLG/SiC would not be prone to σ* energy shifting. However, in order to conclude that this particular methodology of σ* resonance shifts is applicable to SLG/SiC, the substrate effects on SLG/SiC need to be elucidated. Substrate effects had promoted a hard shift in Cu ensembles, and the effects in SiC systems had not been derived. In fact, the value of predicted strain in epitaxial SLG/SiC in Table 1 being higher than 1% is unexpected, suggesting that SiC substrate effects might be more complex than a spectral hard shift.

Indeed, Ferralis reported evidence of structural strain in epitaxial graphene on 6H-SiC(0001), calculated compressive strain at room temperature of 0.8%, associated to long annealing times.[57] The rendered films were under residual compressive strain at room temperature, which again results from a large difference in the thermal expansion coefficients of graphene and SiC. The residual strain has been reported to be tunable by varying the growth time, between the theoretical maximum of almost 0.8% and an empirical minimum value of 0.1%. Following this trend, Schuman et al, reported a compressive strain of 0.2%.[61]

Comparing these available data to value reported here of -1.57%, the prediction for epitaxial SLG/SiC is too high, suggesting the need to account for the specific SiC screening effects in the growth ensemble. To further test the applicability of the calibrated trend in Figure S3 in SI, strain predictions using equation 1 from NEXAFS Carbon K-edge spectra of epitaxially grown

graphene on SiC(Si) found in the literature yielded 0.46%,[62] 0.67%,[63] and 1.07%.[64] Further highlighting the importance of identifying substrate-specific screening effects, these predictions suggest tensile strain in graphene, in opposition to accepted lattice parameter dynamics of epitaxial graphene/SiC that render in reality a compressed epilayer. These results confirm that this methodology will not be applicable to epitaxial SLG/SiC, until impact of substrate effects are accounted for. In particular, substrate screening effects in this system need to be elucidated.

It is worth highlighting that transferred systems do not engage in covalent bonding with the subjacent SiC substrate, and the van der Waals interactions will be weak. Therefore, substrate effects (charge transfer or substrate shielding) will not need to be taken into account here. Although the predicted values for the transferred systems are in excess of the 1% limit identified by Tetlow,[9] these will be highly rippled systems, without substrate pinning effects, which justify the larger values, which are still below 2% compression, and therefore preserving the band structure typical of graphene, as shown in Figure S2 (b). In this scheme, Table 1 shows that transferred systems exhibit larger compressive strain than CVD SLG/Cu, and this increase could be increasing with subsequent transferred layers. Indeed, the initial -0.49% strain in CVD SLG/Cu augments to -1.17% for T-SLG/SiC(Si) and -1.57% for T- 4SLG/SiC(Si). The strained value for T-4SLG/SiC(C) is equal (-1.17%) to that of T-SLG/SiC(Si). In view of these results, transfer seems to augment the frequency and magnitude of rippling events, (as expected) which are subject to be monitored by the σ* shift method discussed here. These data also suggest that transfer of multiple epilayers could have an impact on the level of compressive stress generated, and the dependence on substrate termination is unclear at this time.

Finally, it was mentioned earlier that the microscopy-hyperspectral acquisition mode used here has the ability to characterize segmented regions in each system, applying the σ* shift

method to each one. This would yield not only a strain value for the smaller regions, but an indication of strain variations at wafer level. In this work, only integrated regions of 5×3 mm^2 were analyzed. However, this technology has the capacity to image regions as large as 20×20 mm^2 with a resolution under 10 μm. Hence, the advent of hyperspectral synchrotron spectroscopy paves the way to spatially resolved mechanical deformation at the micron level and wafer scale (which has not been explored here), maintaining molecular sensitivity, and hence, overcoming detectability limits. The procedure highlighted here, demonstrates the methodology needed to curate and process big data in hyperspectral high throughput files in an analytical fashion. Further developments will include the deployment of machine –learning algorithms at different length scales to fully exploit the information derived to inform on mechanical deformation upon growth and processing at industrial scales. In addition, for optimum results, the acquisition needs to be set at the highest energy resolution that the detector and/or spectrometer is capable of. In the present work, most scans have been acquired at 0.2 eV resolution, rather than the maximum 0.06 eV that would yield higher sensitivity in the predicted lattice parameters. For this implementation to come to full term, newly developed hyperspectral NEXAFS detectors need to become forefront technology, accessible in various beamlines. This availability will promote extensive use and exploitation of the technological advancements that this detector portrays.

In essence, this work demonstrates that interfacial substrate interactions can induce measurable changes in the peak positions of NEXAFS resonances, calibrated with the aid of density functional theory calculations, providing a means of mapping strain across transferred graphene samples. In addition, the ability of the σ* shift method to reflect out of plane strain effects has

also been demonstrated. This finding is crucial to account for the ripple-derived strain effects that are known to develop throughout the whole wafer.

Summary and Conclusions

This work proposes a methodology to measure graphene strains at wafer levels using a robust correlation derived from density functional theory calculations and originating from the excitonic nature of σ* and π* resonances. This methodology is directly applicable to CVD-grown graphene on Cu systems as well as to those graphene films that are transferred to substrates with which the established van der Waals interactions are weak. The methodology is also applicable to SiC-derived graphene, although the specifics of substrate interactions need to be elucidated and accounted for. Similarly, this method is applicable to other transmission metal substrates, however, measurements of both charge transfer between graphene and substrate (known to be more prominent than in Cu), as well as substrate screening, are needed to isolate the σ* energy dependence on bond length and strain. The validity of the σ* energy shift correlation with strain rests in the excitonic character of this resonance, having a localized absorbing electron which leads to a core electron decay, being likely the reason for the observed calculations. Importantly, this method holds promise in other 2D materials, probing the bond length directly by measuring a ubiquitous σ* signal, taking into account substrate/epilayer relations as described above. To this end, further work is required to analyze the correlation between functionalization and dimensional reduction.

AUTHOR INFORMATION

Corresponding Author

* evamcampo@gmail.com

Supporting Information has been compiled to delve into the topics discussed in this manuscript. This information is available free of charge via the Internet at http://pubs.acs.org/.

Funding Sources

Project supported by AFOSR Grants FA9550-17-1-0082, FA9550-15-1-0289, and FA9550-14-1-0099 and by the U.S. DOE, Office of Science, Office of Basic Energy Sciences, contract number DEAC02-98CH10886. Computational work was performed in part through High Performance Computing Wales project numbers 095 and 224, as part of the HPCW-Project No. 80621, through European Regional Development Funding and a Fujitsu Fellowship. Simulations of NEXAFS spectra were executed as part of a User Project at the Molecular Foundry, Lawrence Berkeley National Laboratory, which is supported by the Office of Science, Office of Basic Energy Sciences of the U.S. DOE, contract number DE-AC02-05CH11231.

ACKNOWLEDGMENT

EMC was supported by the IR/D program at the National Science Foundation. We thank Dr. Chuong Huynh at Carl Zeiss Microscopy for assistance in Helium Ion Microscopy and Dr. Fahima Ouchen at Air Force Research Laboratory for overseeing graphene processing procedures.

1. Schwierz, F., Graphene transistors. *Nature nanotechnology* **2010,** *5* (7), 487-496.
2. Jain, A.; Ong, S. P.; Hautier, G.; Chen, W.; Richards, W. D.; Dacek, S.; Cholia, S.; Gunter, D.; Skinner, D.; Ceder, G.; Persson, K. A., Commentary: The Materials Project: A materials genome approach to accelerating materials innovation. *APL Materials* **2013,** *1* (1), 011002.
3. Sun, W.; Dacek, S. T.; Ong, S. P.; Hautier, G.; Jain, A.; Richards, W. D.; Gamst, A. C.; Persson, K. A.; Ceder, G., The thermodynamic scale of inorganic crystalline metastability. *Science Advances* **2016,** *2* (11).
4. Novoselov, K. S.; Geim, A. K.; Morozov, S. V.; Jiang, D.; Zhang, Y.; Dubonos, S. V.; Grigorieva, I. V.; Firsov, A. A., Electric Field Effect in Atomically Thin Carbon Films. *Science* **2004,** *306* (5696), 666-669.
5. Avouris, P., Graphene: electronic and photonic properties and devices. *Nano letters* **2010,** *10* (11), 4285-4294.
6. Zhan, B.; Li, C.; Yang, J.; Jenkins, G.; Huang, W.; Dong, X., Graphene Field-Effect Transistor and Its Application for Electronic Sensing. *Small* **2014,** *10* (20), 4042-4065.
7. Couto, N. J.; Costanzo, D.; Engels, S.; Ki, D.-K.; Watanabe, K.; Taniguchi, T.; Stampfer, C.; Guinea, F.; Morpurgo, A. F., Random strain fluctuations as dominant disorder source for high-quality on-substrate graphene devices. *Physical Review X* **2014,** *4* (4), 041019.
8. Hattab, H.; N'Diaye, A. T.; Wall, D.; Klein, C.; Jnawali, G.; Coraux, J.; Busse, C.; van Gastel, R.; Poelsema, B.; Michely, T., Interplay of wrinkles, strain, and lattice parameter in graphene on iridium. *Nano letters* **2012,** *12* (2), 678-682.
9. Tetlow, H.; De Boer, J. P.; Ford, I.; Vvedensky, D.; Coraux, J.; Kantorovich, L., Growth of epitaxial graphene: Theory and experiment. *Physics Reports* **2014,** *542* (3), 195-295.
10. Li, X.; Cai, W.; An, J.; Kim, S.; Nah, J.; Yang, D.; Piner, R.; Velamakanni, A.; Jung, I.; Tutuc, E.; Banerjee, S. K.; Colombo, L.; Ruoff, R. S., Large-area synthesis of high-quality and uniform graphene films on copper foils. *Science* **2009,** *324* (5932), 1312-1314.
11. Mattevi, C.; Kim, H.; Chhowalla, M., A review of chemical vapour deposition of graphene on copper. *Journal of Materials Chemistry* **2011,** *21* (10), 3324-3334.
12. Norimatsu, W.; Kusunoki, M., Epitaxial graphene on SiC {0001}: advances and perspectives. *Physical Chemistry Chemical Physics* **2014,** *16* (8), 3501-3511.
13. Ambrosi, A.; Pumera, M., The CVD graphene transfer procedure introduces metallic impurities which alter the graphene electrochemical properties. *Nanoscale* **2014,** *6* (1), 472-476.
14. Jung, W.; Kim, D.; Lee, M.; Kim, S.; Kim, J. H.; Han, C. S., Ultraconformal contact transfer of monolayer graphene on metal to various substrates. *Advanced Materials* **2014,** *26* (37), 6394-6400.
15. Colombo, L.; Wallace, R. M.; Ruoff, R. S., Graphene growth and device integration. *Proceedings of the IEEE* **2013,** *101* (7), 1536-1556.
16. Zhu, W.; Low, T.; Perebeinos, V.; Bol, A. A.; Zhu, Y.; Yan, H.; Tersoff, J.; Avouris, P., Structure and electronic transport in graphene wrinkles. *Nano letters* **2012,** *12* (7), 3431-3436.
17. Deng, S.; Berry, V., Wrinkled, rippled and crumpled graphene: an overview of formation mechanism, electronic properties, and applications. *Materials Today* **2016,** *19* (4), 197-212.
18. Lee, V.; Park, C.; Jaye, C.; Fischer, D. A.; Yu, Q.; Wu, W.; Liu, Z.; Bao, J.; Pei, S.-S.; Smith, C.; Lysaght, P.; Banerjee, S., Substrate hybridization and rippling of graphene evidenced by near-edge X-ray absorption fine structure spectroscopy. *The Journal of Physical Chemistry Letters* **2010,** *1* (8), 1247-1253.
19. Stöhr, J., *NEXAFS Spectroscopy*. Springer: 2003.

20. Winter, A. D.; Larios, E.; Alamgir, F. M.; Jaye, C.; Fischer, D. A.; Omastova, M.; Campo, E. M., Thermo-active behaviour of ethylene-vinyl acetate | multiwall carbon nanotube composites examined by in situ near edge x-ray absorption fine structure spectroscopy. *The Journal of Physical Chemistry C* **2014,** *118* (7), 3733-3741.
21. Winter, A. D.; Jaye, C.; Fischer, D.; Omastová, M.; Campo, E. M., Prestrain relaxation in non-covalently modified ethylene-vinyl acetate | PyChol | multiwall carbon nanotube nanocomposites. *APL Materials* **2014,** *2* (6), 066105.
22. Winter, A. D.; Larios, E.; Alamgir, F. M.; Jaye, C.; Fischer, D.; Campo, E. M., Near-edge x-ray absorption fine structure studies of electrospun poly (dimethylsiloxane)/poly (methyl methacrylate)/multiwall carbon nanotube composites. *Langmuir* **2013,** *29* (51), 15822-15830.
23. Schultz, B. J.; Patridge, C. J.; Lee, V.; Jaye, C.; Lysaght, P. S.; Smith, C.; Barnett, J.; Fischer, D. A.; Prendergast, D.; Banerjee, S., Imaging local electronic corrugations and doped regions in graphene. *Nature communications* **2011,** *2*, 372.
24. Schultz, B. J.; Jaye, C.; Lysaght, P. S.; Fischer, D. A.; Prendergast, D.; Banerjee, S., On chemical bonding and electronic structure of graphene–metal contacts. *Chemical Science* **2013,** *4* (1), 494-502.
25. Schultz, B. J.; Dennis, R. V.; Lee, V.; Banerjee, S., An electronic structure perspective of graphene interfaces. *Nanoscale* **2014,** *6* (7), 3444-3466.
26. Sheehy, J.; Gil, T.; Winstead, C.; Farren, R.; Langhoff, P., Correlation of molecular valence-and K-shell photoionization resonances with bond lengths. *The Journal of chemical physics* **1989,** *91* (3), 1796-1812.
27. Ni, Z.; Wang, Y.; Yu, T.; Shen, Z., Raman spectroscopy and imaging of graphene. *Nano Research* **2008,** *1* (4), 273-291.
28. Wang, Y. Y.; Ni, Z. H.; Yu, T.; Shen, Z. X.; Wang, H. M.; Wu, Y. H.; Chen, W.; Shen Wee, A. T., Raman studies of monolayer graphene: the substrate effect. *The Journal of Physical Chemistry C* **2008,** *112* (29), 10637-10640.
29. Baio, J. E.; Jaye, C.; Fischer, D. A.; Weidner, T., Multiplexed Orientation and Structure Analysis by Imaging Near-Edge X-ray Absorption Fine Structure (MOSAIX) for Combinatorial Surface Science. *Analytical chemistry* **2013,** *85* (9), 4307-4310.
30. Konicek, A.; Jaye, C.; Hamilton, M.; Sawyer, W.; Fischer, D.; Carpick, R., Near-Edge X-ray Absorption Fine Structure Imaging of Spherical and Flat Counterfaces of Ultrananocrystalline Diamond Tribological Contacts: A Correlation of Surface Chemistry and Friction. *Tribology Letters* **2011,** *44* (1), 99-106.
31. Avila, J.; Razado, I.; Lorcy, S.; Fleurier, R.; Pichonat, E.; Vignaud, D.; Wallart, X.; Asensio, M. C., Exploring electronic structure of one-atom thick polycrystalline graphene films: A nano angle resolved photoemission study. *Scientific reports* **2013,** *3*.
32. Winter, A. D.; Rojas, W. Y.; Williams, A. D.; Kim, S. S.; Ouchen, F.; Fischer, D. A.; Weiland, C.; Principe, E.; Banerjee, S.; Huynh, C., Monitoring Deformation in Graphene Through Hyperspectral Synchrotron Spectroscopy to Inform Fabrication. *The Journal of Physical Chemistry C* **2017,** *121* (29), 15653-15664.
33. Kasry, A.; Kuroda, M. A.; Martyna, G. J.; Tulevski, G. S.; Bol, A. A., Chemical doping of large-area stacked graphene films for use as transparent, conducting electrodes. *ACS nano* **2010,** *4* (7), 3839-3844.
34. Latil, S.; Henrard, L., Charge carriers in few-layer graphene films. *Physical Review Letters* **2006,** *97* (3), 036803.

35. Bae, S.; Kim, H.; Lee, Y.; Xu, X.; Park, J.-S.; Zheng, Y.; Balakrishnan, J.; Lei, T.; Kim, H. R.; Song, Y. I., Roll-to-roll production of 30-inch graphene films for transparent electrodes. *Nature nanotechnology* **2010,** *5* (8), 574-578.
36. Kim, S. S.; Kuang, Z.; Ngo, Y. H.; Farmer, B. L.; Naik, R. R., Biotic–Abiotic Interactions: Factors that Influence Peptide–Graphene Interactions. *ACS Appl. Mater. Interfaces* **2015,** *7* (36), 20447-20453.
37. Seah, M. P.; Dench, W. A., Quantitative electron spectroscopy of surfaces: A standard data base for electron inelastic mean free paths in solids. *Surface and interface analysis* **1979,** *1* (1), 2-11.
38. Genzer, J.; Kramer, E. J.; Fischer, D. A., Accounting for Auger yield energy loss for improved determination of molecular orientation using soft x-ray absorption spectroscopy. *Journal of applied physics* **2002,** *92* (12), 7070-7079.
39. Kohn, W.; Sham, L. J., Self-consistent equations including exchange and correlation effects. *Physical Review* **1965,** *140* (4A), A1133.
40. Giannozzi, P.; Baroni, S.; Bonini, N.; Calandra, M.; Car, R.; Cavazzoni, C.; Ceresoli, D.; Chiarotti, G. L.; Cococcioni, M.; Dabo, I., QUANTUM ESPRESSO: a modular and open-source software project for quantum simulations of materials. *Journal of Physics: Condensed Matter* **2009,** *21* (39), 395502.
41. Perdew, J. P.; Zunger, A., Self-interaction correction to density-functional approximations for many-electron systems. *Physical Review B* **1981,** *23* (10), 5048.
42. Perdew, J. P.; Burke, K.; Ernzerhof, M., Generalized gradient approximation made simple. *Physical review letters* **1996,** *77* (18), 3865.
43. Fuentes-Cabrera, M.; Baskes, M. I.; Melechko, A. V.; Simpson, M. L., Bridge structure for the graphene/Ni (111) system: a first principles study. *Physical Review B* **2008,** *77* (3), 035405.
44. Xu, Z.; Buehler, M. J., Interface structure and mechanics between graphene and metal substrates: a first-principles study. *Journal of Physics: Condensed Matter* **2010,** *22* (48), 485301.
45. Olsen, T.; Yan, J.; Mortensen, J. J.; Thygesen, K. S., Dispersive and covalent interactions between graphene and metal surfaces from the random phase approximation. *Physical review letters* **2011,** *107* (15), 156401.
46. Prendergast, D.; Galli, G., X-Ray Absorption Spectra of Water from First Principles Calculations. *Phys. Rev. Lett.* **2006,** *96* (21), 215502.
47. Pedio, M.; Giglia, A.; Mahne, N.; Nannarone, S.; Giovannini, S.; Cepek, C.; Boscherini, F.; Carboni, R.; Benfatto, M.; Della Longa, S., C k-edge NEXAFS of 6H-SiC and 3C-SiC systems. *Physica Scripta* **2005,** *2005* (T115), 308.
48. Banerjee, S.; Hemraj-Benny, T.; Wong, S. S., Covalent surface chemistry of single-walled carbon nanotubes. *Advanced Materials* **2005,** *17* (1), 17-29.
49. Bell, D. C.; Lemme, M. C.; Stern, L. A.; Williams, J. R.; Marcus, C. M., Precision cutting and patterning of graphene with helium ions. *Nanotechnology* **2009,** *20* (45), 455301.
50. Campo, E. M.; Larios, E.; Huynh, C.; Ananth, M., Helium ion microscopy of electrospun CNT–polymer composites. *Journal of Materials Research* **2015,** *30* (01), 130-140.
51. Piancastelli, M. N.; Lindle, D. W.; Ferrett, T. A.; Shirley, D. A., The relationship between shape resonances and bond lengths. *The Journal of chemical physics* **1987,** *86* (5), 2765-2771.

52. Hitchcock, A. P.; Stöhr, J., K-shell shape resonances and intramolecular bond lengths. Comments on ''The relationship between shape resonances and bond lengths''. *The Journal of chemical physics* **1987,** *87* (5), 3253-3255.
53. Lee, V.; Dennis, R. V.; Schultz, B. J.; Jaye, C.; Fischer, D. A.; Banerjee, S., Soft x-ray absorption spectroscopy studies of the electronic structure recovery of graphene oxide upon chemical defunctionalization. *The Journal of Physical Chemistry C* **2012,** *116* (38), 20591-20599.
54. Ågren, H.; Vahtras, O.; Carravetta, V., Near-edge core photoabsorption in polyacenes: model molecules for graphite. *Chemical physics* **1995,** *196* (1-2), 47-58.
55. Brühwiler, P. A.; Maxwell, A. J.; Puglia, C.; Nilsson, A.; Andersson, S.; Mårtensson, N., π * and σ * Excitons in C 1 s Absorption of Graphite. *Physical review letters* **1995,** *74* (4), 614.
56. Gui, G.; Li, J.; Zhong, J., Band structure engineering of graphene by strain: first-principles calculations. *Physical Review B* **2008,** *78* (7), 075435.
57. Ferralis, N.; Maboudian, R.; Carraro, C., Evidence of structural strain in epitaxial graphene layers on 6H-SiC (0001). *Physical review letters* **2008,** *101* (15), 156801.
58. Chaitoglou, S.; Bertrán, E., Control of the Strain in CVD Grown Graphene Over Copper via the H2 Flow. *The Journal of Physical Chemistry C* **2016**.
59. He, R.; Zhao, L.; Petrone, N.; Kim, K. S.; Roth, M.; Hone, J.; Kim, P.; Pasupathy, A.; Pinczuk, A., Large physisorption strain in chemical vapor deposition of graphene on copper substrates. *Nano letters* **2012,** *12* (5), 2408-2413.
60. Coletti, C.; Riedl, C.; Lee, D. S.; Krauss, B.; Patthey, L.; von Klitzing, K.; Smet, J. H.; Starke, U., Charge neutrality and band-gap tuning of epitaxial graphene on SiC by molecular doping. *Physical Review B* **2010,** *81* (23), 235401.
61. Schumann, T.; Dubslaff, M.; Oliveira Jr, M. H.; Hanke, M.; Lopes, J. M. J.; Riechert, H., Effect of buffer layer coupling on the lattice parameter of epitaxial graphene on SiC (0001). *Physical Review B* **2014,** *90* (4), 041403.
62. Aristov, V. Y.; Urbanik, G.; Kummer, K.; Vyalikh, D. V.; Molodtsova, O. V.; Preobrajenski, A. B.; Zakharov, A. A.; Hess, C.; Hänke, T.; Buchner, B., Graphene synthesis on cubic SiC/Si wafers. Perspectives for mass production of graphene-based electronic devices. *Nano letters* **2010,** *10* (3), 992-995.
63. Kim, K.-j.; Choi, J.; Lee, H.; Lee, H.-K.; Kang, T.-H.; Han, Y.-H.; Lee, B.-C.; Kim, S.; Kim, B., Effects of 1 MeV electron beam irradiation on multilayer graphene grown on 6H-SiC (0001). *The Journal of Physical Chemistry C* **2008,** *112* (34), 13062-13064.
64. Kim, K.-j.; Lee, H.; Choi, J.; Lee, H.; Kang, T.; Kim, B.; Kim, S., Temperature dependent structural changes of graphene layers on 6H-SiC (0001) surfaces. *Journal of Physics: Condensed Matter* **2008,** *20* (22), 225017.

Table of Contents Figure

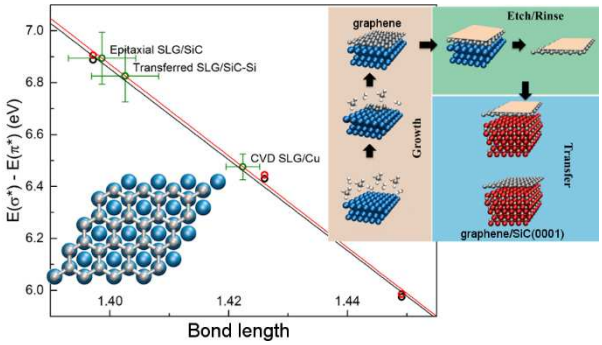
Epitaxial SLG/SiC
Transferred SLG/SiC-Si
CVD SLG/Cu
E(σ*) - E(π*) (eV)
Bond length
graphene
Growth
Etch/Rinse
Transfer
graphene/SiC(0001)